IEEE Access
Multidisciplinary | Rapid Review | Open Access Journal

Received 8 May 2023, accepted 11 June 2023, date of publication 19 June 2023, date of current version 10 July 2023.

Digital Object Identifier 10.1109/ACCESS.2023.3287220

RESEARCH ARTICLE

Sensorless Control and Inductances Estimation of IPMSMs Using FPGA and High Bandwidth Current Measurement

M. X. BUI[1], (Member, IEEE), DAN XIAO[2], AND M. FAZ RAHMAN[2], (Life Fellow, IEEE)

[1]Faculty of Control Engineering, Le Quy Don Technical University, Ha Noi 11917, Vietnam
[2]School of Electrical Engineering and Telecommunications, University of New South Wales, Kensington, NSW 2052, Australia

Corresponding author: M. X. Bui (minh.buixuan@ieee.org)

This work was supported by the Nafosted Vietnam under Grant 107.99-2019.341.

ABSTRACT This paper presents a sensorless control method and a very fast on-line inductances identification of an IPMSM. The current slopes (derivatives) at one active-voltage vector and one zero-voltage vector are measured every PWM cycle to estimate the rotor speed and position with the aim of increasing the estimation accuracy and reducing total harmonic distortion of the phase currents. In addition to these current slopes, the DC bus voltage of the inverter is measured to estimate the machine inductances on-line. The proposed on-line parameter identification method can overcome the drawback of the existing off-line methods, such as: the requirement of a robust mechanical clamping system and test signal generators. The proposed on-line method also addresses the limit of the existing on-line methods, such as slow update and the possibility of incorrect convergence of the estimated parameters. Extensive experimental studies were conducted to verify the effectiveness and robustness of the proposed sensorless control and parameters identification of the IPMSM.

INDEX TERMS Sensorless control, on-line parameter identification, current derivative measurement, IPMSM.

I. INTRODUCTION

Interior Permanent magnet synchronous motors (IPMSM) have been applied widely in high performance applications due to their high power density, high efficiency and high control performance. The elimination of mechanical sensor, such as encoder or resolver can help to improve the reliability, reduce the size and cost of the control system [1]. So far, the sensorless control methods can be classified into two main categories. The first category is based on the dynamic model of the IPMSM. The rotor speed and position can be estimated based on the estimation of back EMF [2], [3], [4] or stator flux [5], [6]. In general, these methods utilize the parameters of the machine model, such as stator resistance, d-q axis inductances in the development of the estimation model of the rotor speed and position. Therefore, the variation of machine parameters during the operation, such as magnetic saturation affects the performance of these model-based estimators. In addition, during low and very low speed operations these methods lose their robustness due to low signal to noise ratio. The second category is based on the saliency machine inductances in d- and q- axes, such as square wave signal injections [7], [8], pulse signal injections [9], [10]. These methods inject a high frequency signal to the machine and estimate the rotor speed and position by processing of the high frequency response of the phase current. In general, these methods are robust at low and very low speed operation since they are independent of machine model. However, at high and very high speeds, the operating speeds are limited by the modulation index. The other drawbacks of saliency-based methods are the noise, high current and torque ripple due

The associate editor coordinating the review of this manuscript and approving it for publication was Zhuang Xu.

to the injected signal. In order to reduce the noise and current ripples, the methods based on the measurement of current slopes (derivatives) during the excitation of the voltage vector of the standard pulse width modulation have been proposed [11], [12], [13]. These methods do not use any injected signal, instead utilize the voltage vector during normal PWM as the excitation signals. However, due to the parasitic effect, the phase current oscillates at high frequency after the switching transition, hence affecting the accuracy of the current slope measurement. For the IPMSM with high inductance, this oscillation time could last for about 20 microseconds at full load condition. Therefore, the extension and compensation of the voltage vector must be required. For the conventional fundamental PWM excitation (FPE) method, the current derivatives at two active voltage vector and two zero voltage vector are measured to estimate rotor speed and position [12]. For IPMSM with high inductance, the long extension of the two active voltage vectors and two zero voltage vectors are required, thus increasing the total harmonic distortion of the phase current and limiting the maximum operating speed. In order to reduce the total harmonic distortion and increase the sensorless operating speed range, this paper proposes a method to estimate the rotor speed and current of the IPMSM by using current slopes at only one active and one zero voltage vector.

It is worth noting that the inductances of the IPMSM have a close relationship with the phase current slopes during the excitation of active and zero voltage vectors. This paper also presents a very fast online method to estimate the d- and q- axis inductances based on the measurement of the current slopes and the DC bus voltage of the three phases two levels converter. This proposed method can handle the disadvantages of the off-line methods which require a rigid mechanical clamping system, the power signal generator or the mover to rotate the rotor to a certain speed. Additionally, the proposed method can overcome the weaknesses of the on-line methods based on the machine model shown in [14], [15], [16], [17], and [18]. The weaknesses of these methods are the sensitivity to the non-linearity of the converter, slow update of the estimated parameters due to the recursive principles, the possibility of divergence of the algorithm, and the complexity of tuning the hyperparameters of the method.

Extensive numerical simulation and experimental study have been conducted to verify the effectiveness and robustness of the proposed sensorless control method over a full speed range from zero to rated speed and the inductances estimation methods. The conventional FPE sensorless method was used as a benchmark to evaluate the proposed methods in terms of estimation accuracy and total harmonic distortion of the phase current. The performance of the proposed inductance estimation method was compared with the off-line method in term of estimation accuracy, and with the recursive least square online methods in terms of parameter updating time.

II. PROPOSED SENSORLESS CONTROL AND INDUCTANCE ESTIMATION

A. IPMSM DYNAMIC MODEL

The three-phase model of the IPMSM can be described as:

$$\begin{aligned} V_A &= R_A i_A + \frac{d}{dt}(L_{AA} i_A + L_{AB} i_B + L_{AC} i_C + \lambda_f cos\theta_e) \\ V_B &= R_B i_B + \frac{d}{dt}(L_{BA} i_A + L_{BB} i_B + L_{BC} i_C \\ &\quad + \lambda_f \cos(\theta_e - 2\pi/3)) \\ V_C &= R_C i_C + \frac{d}{dt}(L_{CA} i_A + L_{CB} i_B + L_{CC} i_C \\ &\quad + \lambda_f \cos(\theta_e - 4\pi/3)) \end{aligned} \tag{1}$$

where V_A, V_B, V_C are stator voltage of phase A, B and C, respectively; i_A, i_B, i_C are the stator current of phase A, B, and C, respectively; R_A, R_B, R_C are the stator resistance of phase A, B, and C respectively; θ_e is the electrical angle of the rotor; λ_f is the permanent magnet flux linkage; L_{AA}, L_{BB}, L_{CC} are the stator self-inductance of phase A, B and C respectively; L_{AB}, L_{BA}, L_{AC}, L_{CA}, L_{BC}, L_{CB} are the mutual inductances between respective phases.

$$\begin{aligned} L_{AA} &= L_\Sigma + L_\Delta \cos(2\theta_e) \\ L_{BB} &= L_\Sigma + L_\Delta \cos(2\theta_e + 2\pi/3) \\ L_{CC} &= L_\Sigma + L_\Delta \cos(2\theta_e + 4\pi/3) \\ L_{BC} &= L_{CB} = -\frac{L_\Sigma}{2} + L_\Delta \cos(2\theta_e) \\ L_{AB} &= L_{BA} = -\frac{L_\Sigma}{2} + L_\Delta \cos(2\theta_e - 2\pi/3) \\ L_{AC} &= L_{CA} = -\frac{L_\Sigma}{2} + L_\Delta \cos(2\theta_e - 4\pi/3) \\ L_\Sigma &= \frac{L_{di} + L_{qi}}{3}; \quad L_\Delta = \frac{L_{di} - L_{qi}}{3} \end{aligned} \tag{2}$$

where $L_\sum$, L_Δ are the average inductance and the magnitude of the inductance variation; L_{di}, L_{qi} are direct and quadrature incremental inductances respectively.

Assume that during a PWM cycle, the rotor angle of the machine is unchanged, thus the self and mutual inductance are unchanged. (1) can be rewritten as:

$$\begin{aligned} V_A &= R_A i_A + L_{AA}\frac{di_A}{dt} + L_{AB}\frac{di_B}{dt} + L_{AC}\frac{di_C}{dt} + e_A \\ V_B &= R_B i_B + L_{BA}\frac{di_A}{dt} + L_{BB}\frac{di_B}{dt} + L_{BC}\frac{di_C}{dt} + e_B \\ V_C &= R_C i_C + L_{CA}\frac{di_A}{dt} + L_{CB}\frac{di_B}{dt} + L_{CC}\frac{di_C}{dt} + e_C \end{aligned} \tag{3}$$

where e_A, e_B, e_C are back EMF of phase A, B and C, respectively.

B. ESTIMATION OF ROTOR SPEED AND POSITION BASED ON CURRENT SLOPES

Scalars of the position vector are defined as:

$$\begin{aligned} p_A &= \frac{2L_\Delta}{L_\Sigma}\cos(2\theta_e) \\ p_B &= \frac{2L_\Delta}{L_\Sigma}\cos(2\theta_e - \frac{2\pi}{3}) \\ p_C &= \frac{2L_\Delta}{L_\Sigma}\cos(2\theta_e - \frac{4\pi}{3}) \end{aligned} \tag{4}$$

These scalars of the position vector can be calculated based on the phase current slopes at one active and one zero voltage vector as shown in Table 1 [19]. The subscript of the equations in Table 1 indicates the voltage vector where the current slopes are measured. The quantity g in the equations in Table 1 can be shown as the function of the DC bus voltage (V_{DC}), average inductance and the magnitude of the inductance variation as followed:

$$g = \frac{9}{2V_{DC}}(L_\Sigma)\left(1 - \left(\frac{L_\Delta}{L_\Sigma}\right)^2\right) \tag{5}$$

Quantity g can be calculated based on the current slopes at two active and one zero voltage vector as shown in Table 2 by assuming the negligible variation of the rotor position during two consecutive PWM cycles [19].

The scalars p_α, p_β of the position vector in the stationary reference frame can be expressed as:

$$\begin{aligned} p_\alpha &= \frac{2p_A - p_B - p_C}{3} = \frac{2L_\Delta}{L_\Sigma}\cos(2\theta_e) \\ p_\beta &= \frac{p_B - p_C}{\sqrt{3}} = -\frac{2L_\Delta}{L_\Sigma}\sin(2\theta_e) \end{aligned} \tag{6}$$

The phase lock loop (PLL) is then used to estimate rotor speed and position. The design details of this PLL is shown in [20].

C. ESTIMATION OF INCREMENTAL AND APPARENT MACHINE INDUCTANCES

The incremental inductances of the machine can be found by solving (5) and (6):

$$L_{qi} = \frac{gV_{DC}}{3\left(1 - \frac{\sqrt{p_\alpha^2+p_\beta^2}}{2}\right)}; \quad L_{di} = \frac{gV_{DC}}{3\left(1 + \frac{\sqrt{p_\alpha^2+p_\beta^2}}{2}\right)} \tag{7}$$

By taking the integral of the incremental inductance, the apparent inductance of the machine can be obtained as:

$$\begin{aligned} L_d^{(n)} &= \frac{\Phi_d^{(n)}}{I_d^{(n)}} = \frac{\sum_{k=1}^{n} L_{di}^{(k)}\left(I_d^{(k)} - I_d^{(k-1)}\right)}{I_d^{(n)}} \\ L_q^{(n)} &= \frac{\Phi_q^{(n)}}{I_q^{(n)}} = \frac{\sum_{k=1}^{n} L_{qi}^{(k)}\left(I_q^{(k)} - I_q^{(k-1)}\right)}{I_q^{(n)}} \end{aligned} \tag{8}$$

where $L_d^{(n)}, L_q^{(n)}$ are the d- and q- axes apparent inductances, respectively; $\Phi_d^{(n)}$, $\Phi_q^{(n)}$ are the d- and q- axes total fluxes, respectively; $L_{di}^{(k)}, L_{qi}^{(k)}$ are the d- and q- incremental inductances calculated from (7), respectively; $I_d^{(k)}, I_q^{(k)}$ is the d- and q- current, respectively; n is the number of current values from zero to the operating level. The accepted resolution of the discrete integration in (8) is determined by n. For this study, each integration step is 0.1A.

It is noted that the update of quantity g in Table 2 determines how fast the estimated inductances are updated. By measuring the current derivatives two active- and one-zero voltage vectors during each PWM cycle, quantity g and the estimated inductances can be updated at the switching frequency [21].

TABLE 1. Position scalars of IPMSM with star connection.

Active and zero-voltage vector	p_A	p_B	p_C
V_1 and V_0	$2-g\left(\frac{di_A^{(1)}}{dt}-\frac{di_A^{(0)}}{dt}\right)$	$-1-g\left(\frac{di_C^{(1)}}{dt}-\frac{di_C^{(0)}}{dt}\right)$	$-1-g\left(\frac{di_B^{(1)}}{dt}-\frac{di_B^{(0)}}{dt}\right)$
V_2 and V_0	$-1+g\left(\frac{di_B^{(2)}}{dt}-\frac{di_B^{(0)}}{dt}\right)$	$-1+g\left(\frac{di_A^{(2)}}{dt}-\frac{di_A^{(0)}}{dt}\right)$	$2+g\left(\frac{di_C^{(2)}}{dt}-\frac{di_C^{(0)}}{dt}\right)$
V_3 and V_0	$-1-g\left(\frac{di_C^{(3)}}{dt}-\frac{di_C^{(0)}}{dt}\right)$	$2-g\left(\frac{di_B^{(3)}}{dt}-\frac{di_B^{(0)}}{dt}\right)$	$-1-g\left(\frac{di_A^{(3)}}{dt}-\frac{di_A^{(0)}}{dt}\right)$
V_4 and V_0	$2+g\left(\frac{di_A^{(4)}}{dt}-\frac{di_A^{(0)}}{dt}\right)$	$-1+g\left(\frac{di_C^{(4)}}{dt}-\frac{di_C^{(0)}}{dt}\right)$	$-1+g\left(\frac{di_B^{(4)}}{dt}-\frac{di_B^{(0)}}{dt}\right)$
V_5 and V_0	$-1-g\left(\frac{di_B^{(5)}}{dt}-\frac{di_B^{(0)}}{dt}\right)$	$-1-g\left(\frac{di_A^{(5)}}{dt}-\frac{di_A^{(0)}}{dt}\right)$	$2-g\left(\frac{di_C^{(5)}}{dt}-\frac{di_C^{(0)}}{dt}\right)$
V_6 and V_0	$-1+g\left(\frac{di_C^{(6)}}{dt}-\frac{di_C^{(0)}}{dt}\right)$	$2+g\left(\frac{di_B^{(6)}}{dt}-\frac{di_B^{(0)}}{dt}\right)$	$-1+g\left(\frac{di_A^{(6)}}{dt}-\frac{di_A^{(0)}}{dt}\right)$

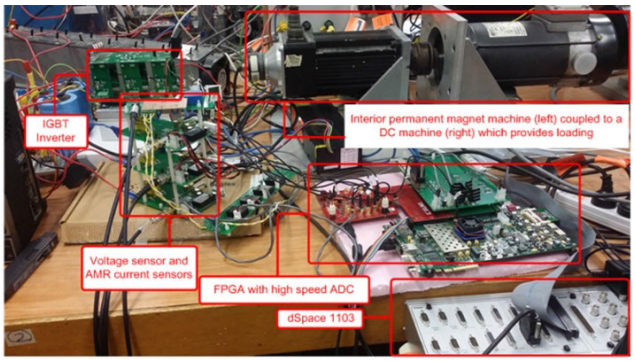

FIGURE 1. Experimental setup.

III. EXPERIMENTAL SETUP AND RESULTS

A. EXPERIMENTAL SETUP

As shown in Fig. 1, the experimental setup includes one tested IPMSM, of which the parameters are shown in Table 3. This machine is loaded by the DC motor and the H-bridge. The dSPACE1103 is used to implement the Direct Torque and Flux Control (DTFC) scheme, estimate the rotor speed and position, and the machine inductances. The Anisotropic

TABLE 2. Calculation of *g*.

Active-voltage vectors	*g*
V_1 and V_2	$\frac{3}{\frac{di_A^{(1)}}{dt}-\frac{di_A^{(0)}}{dt}+\frac{di_B^{(2)}}{dt}-\frac{di_B^{(0)}}{dt}}$
V_2 and V_3	$\frac{3}{\frac{di_A^{(2)}}{dt}-\frac{di_A^{(0)}}{dt}+\frac{di_B^{(3)}}{dt}-\frac{di_B^{(0)}}{dt}}$
V_3 and V_4	$\frac{-3}{\frac{di_A^{(4)}}{dt}-\frac{di_A^{(0)}}{dt}+\frac{di_C^{(3)}}{dt}-\frac{di_C^{(0)}}{dt}}$
V_4 and V_5	$\frac{-3}{\frac{di_A^{(4)}}{dt}-\frac{di_A^{(0)}}{dt}+\frac{di_B^{(5)}}{dt}-\frac{di_B^{(0)}}{dt}}$
V_5 and V_6	$\frac{-3}{\frac{di_A^{(5)}}{dt}-\frac{di_A^{(0)}}{dt}+\frac{di_B^{(6)}}{dt}-\frac{di_B^{(0)}}{dt}}$
V_6 and V_1	$\frac{3}{\frac{di_A^{(1)}}{dt}-\frac{di_A^{(0)}}{dt}+\frac{di_C^{(6)}}{dt}-\frac{di_C^{(0)}}{dt}}$

Magneto-Resistive (AMR) current sensor CMS3005 is used to sense the phase currents. Three Analog to Digital Converter (ADC) 12bits and Field Programable Gate Array (FPGA) ML605 are used to sample the currents from current sensors, estimate the current slopes during every modulated voltage vector and also generate the PWM signals. The block diagram of the sensorless control and inductance estimation is presented in Fig. 2.

B. CURRENT SLOPE MEASUREMENT

The current slopes are measured by using the least square algorithm:

$$\frac{di}{dt}=\frac{n\sum_{i=1}^{n}x_iy_i-\sum_{i=1}^{n}x_i\sum_{i=1}^{n}y_i}{n\sum_{i=1}^{n}x_i^2-(\sum_{i=1}^{n}x_i)^2} \tag{9}$$

where x_i and y_i represents time and the current sample respectively; n is the number of total samplings.

In order to handle the effect of common-mode noise, the high bandwidth current sensors (AMR sensor with the bandwidth of about 2 MHz), high-speed ADCs (50 MSPS) and the RC filter have been utilized. Moreover, the sampling of the current waveforms is delayed until the oscillations in current die out after the switching transition. The duration of high frequency oscillation of the phase current after switching transition for the tested IPMSM (about 20 μs under full load) is far longer than that of the PMSM (about 8μs). Therefore, the sampling of the phase current is delayed by 20 μs after switching transition. A minimum of pulse width (*psmin*) of 24 μs was implemented in order to obtain at least 200 current samples for di/dt calculation, which can guarantee the satisfactory accuracy of current derivative measurement.

TABLE 3. Parameters of IPMSMs tested and control system.

Number of pole pair	2
Stator resistance	5.8 Ω
Magnet flux linkage	0.533 Wb
d-axis inductance	0.0448 H
q-axis inductance	0.1024 H
Phase voltage (RMS)	230 V
Phase current (RMS)	3 A
Rated torque	6 Nm
Rated speed	1500 rpm
Switching frequency	5 kHz
Sampling rate of ADCs	50 MSPS
psmin	24 µs

C. EXPERIMENTAL RESULTS OF THE PROPOSED SENSORLESS CONTROL METHOD

The proposed sensorless control method is compared with the conventional FPE method [13] in terms of estimation accuracy and the total harmonic distortion of the phase currents.

Fig. 3 shows the experimental results of the proposed method and the conventional FPE method when the machine operates at 50 rpm under 5.5 Nm (90% of rated torque). Fig. 3 shows the operation load torque (Machine torque), reference speed (Speed ref), the actual speed (Speed enc), the estimated speed by the proposed method (Speed est), the current slopes of phase A at the first and second active voltage vector (di/dt at V1 and di/dt at V2), and the position estimation error in electrical degree from top to bottom, respectively.

It is obvious that the proposed sensorless method results in the position error within 5 electrical degrees, which is 4 times smaller than the position error (within 20 electrical degrees) resulted by the conventional FPE method. The better accuracy of the proposed method at low speeds can be explained that the more accurate current slopes at the first active voltage vector than at the second active voltage vector are used to estimate the rotor speed and position. In contrast, the conventional FPE method utilizes the current slopes at both first and second active voltage vector during the first haft of a PWM cycle.

The performance of the proposed sensorless method at zero speed under 83% of rated load (5Nm) reversal is presented in Fig. 4. The first plot shows the machine torque in Nm; the second plot shows the actual position (Position enc) and the estimated position (Position est); the third plot presents the position estimation error between the actual position and the estimated position; the fourth plot shows speed reference (Speed ref), actual speed (Speed enc) and estimated speed (Speed est); The last plot shows the speed estimation error between the actual speed and the estimated speed.

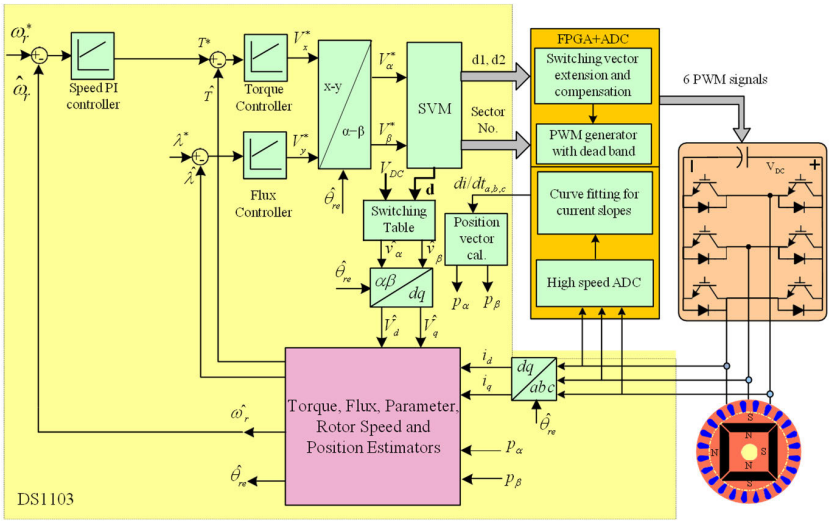

FIGURE 2. The block diagram of the proposed sensorless and inductance estimation system.

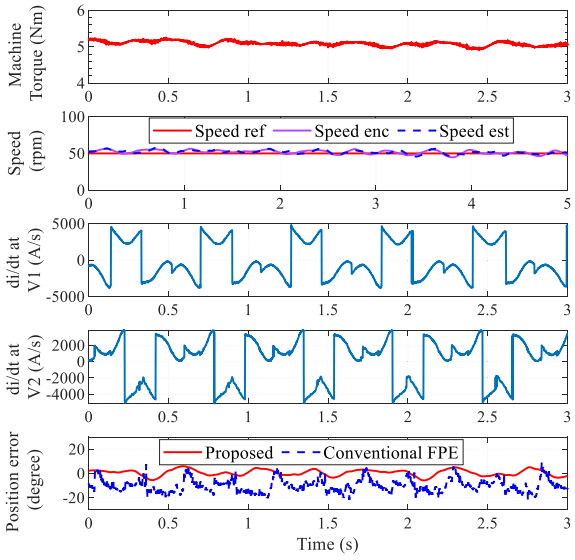

FIGURE 3. Experimental results of two sensorless methods at 50 rpm under 90% of rated load (experiment).

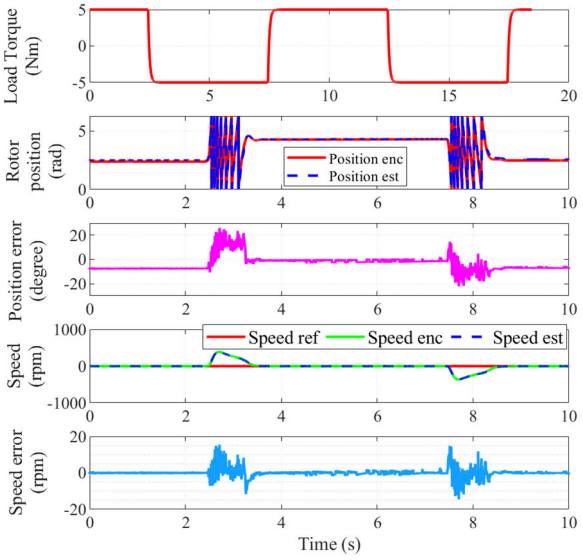

FIGURE 4. Performance of the proposed sensorless method at zero speed under 83% of rated load reversal (experiment).

It is noted that during the transient, the speed increases to the peak of about 400 rpm; the estimated speed error is within 15 rpm; and the position estimation error is within 25 electrical degrees. During the steady state at zero speed, the position estimation error is within 8 electrical degrees, while the speed estimation error is within 1 rpm.

The performance of the proposed sensorless method with rated speed reversal under no load condition is presented in Fig. 5. It is obvious that the position estimation errors during the transient and steady state are within 30 electrical degrees and 5 electrical degrees, respectively.

Fig. 6 compares the total harmonic distortion (THD) of the phase currents between the proposed sensorless method and the conventional FPE method over the full speed range from zero to rated speed under half load. In general, the total harmonic distortion caused by the proposed method is lower than the total harmonic distortion caused by the conventional FPE method. Especially, at high speed operation the THD of the conventional FPE method is much higher than the proposed method. As an example, at 1500 rpm the THD of the proposed method (2.2%) is about a half of the THD of the conventional FPE method (4.5%). This is explained by the extension of more voltage vectors of the conventional FPE method compared to the proposed methods.

D. SIMULATION AND EXPERIMENTAL RESULTS OF THE PROPOSED ON-LINE METHOD FOR ESTIMATING MACHINE INDUCTANCES

The proposed inductance estimation method has been verified by simulation and experimental study. Fig. 7 and Fig. 8 present the performance of the proposed inductance estima-

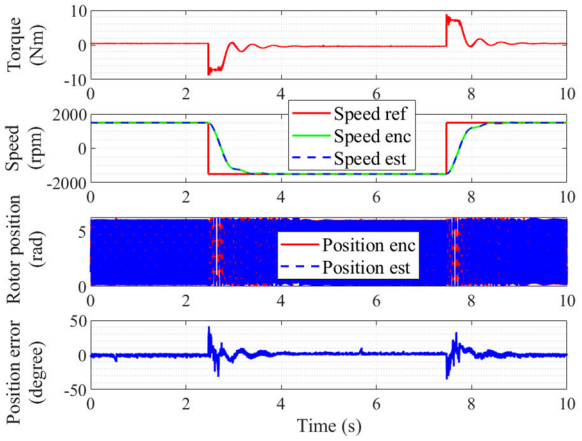

FIGURE 5. Performance of the proposed sensorless method with speed reversal at 1500 rpm under no load condition (experiment).

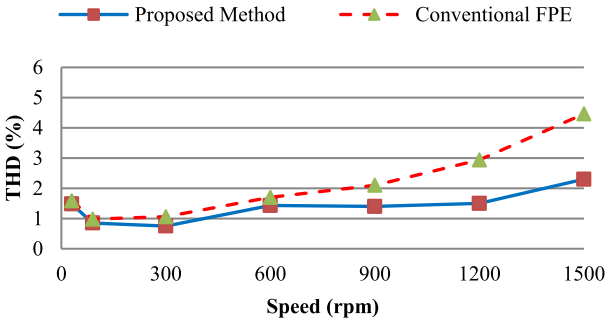

FIGURE 6. Total Harmonic Distortion under 50% of rated torque (experiment).

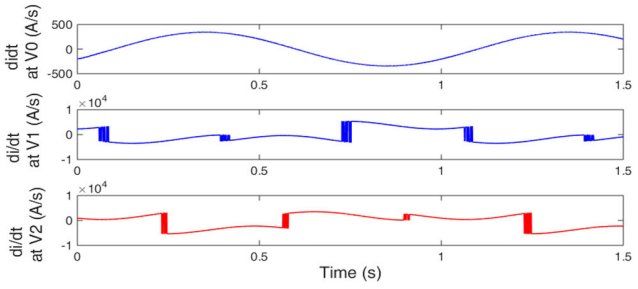

FIGURE 7. Current derivatives for inductance estimation at 30 rpm under full load (simulation).

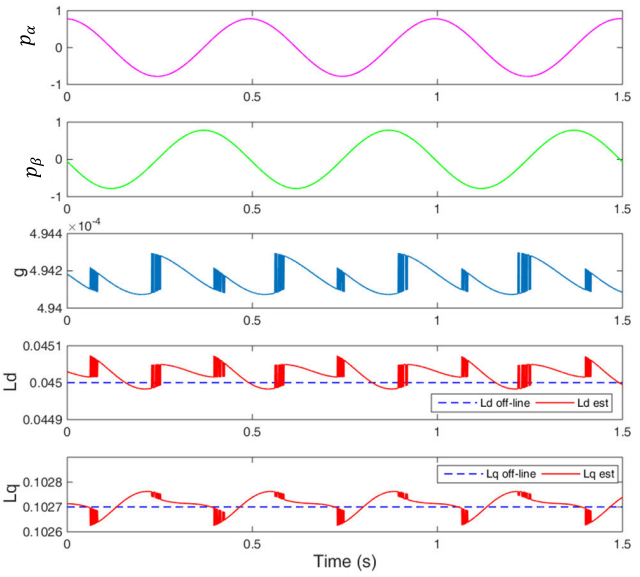

FIGURE 8. Inductance estimation at 30 rpm under full load (simulation).

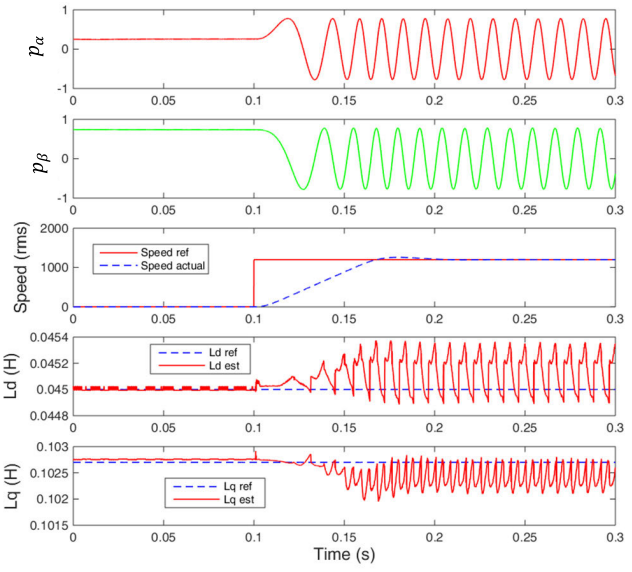

FIGURE 9. Inductances estimation with speed acceleration from zero to 1200 rpm under full load (simulation).

tion method when the machine operates at 30 rpm under full load condition. In this loading condition the machine torque is 6 Nm and the RMS phase current is 2.5 A. The off-line measured L_d and L_q are 0.045H and 0.1027H respectively.

Fig. 7 shows the current slopes at the zero-voltage vector, the first active-voltage vector and the second active-voltage vector of phase A during each PWM cycle. These current slopes are used to calculate the positional vector and g in Table 2 and 3.

Fig. 8 demonstrates the positional scalars, p_α, p_β and g which are used to estimate machine inductances as shown in (7). Fig. 8 also compares the estimated inductances (Ld est, Lq est) with the off-line measured ones (Ld offline, Lq offline), which are set to be the inductances of the IPMSM model. It is obvious that the errors between estimated inductances and the corresponding inductances of the IPMSM model are smaller than 0.1 mH.

Fig. 9 shows the performance of the proposed method when the IPMSM accelerates from zero speed to 1200 rpm under full load condition. The off-line measured inductances at full load condition are set in the IPMSM model (L_d = 0.045 H and L_q = 0.1027H). It is obvious that during the steady state and transient state, the estimated inductances follow closely to the reference inductances. The error between the estimated and the references L_d is smaller than 0.4 mH, while the error between the estimated and the references L_q is smaller than 0.7 mH.

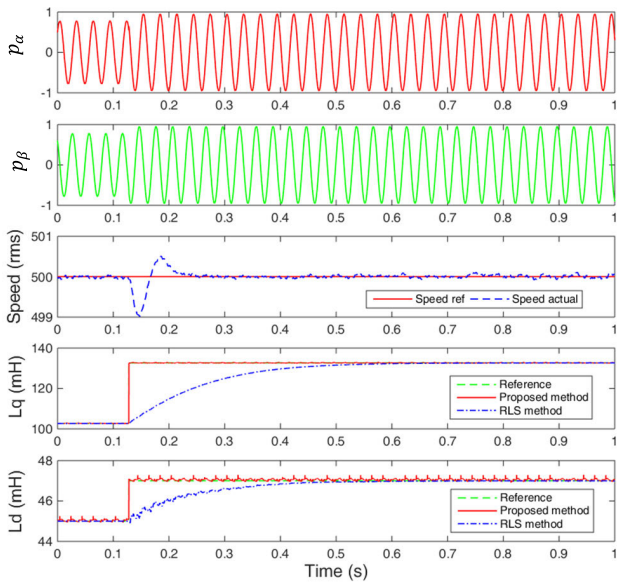

FIGURE 10. Inductances estimation of the proposed- and RLS based-methods (simulation).

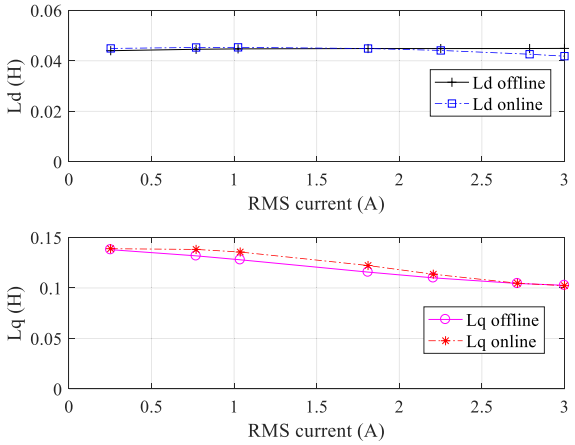

FIGURE 11. On-line estimation of inductances at 300 rpm (experiment).

Fig. 10 compares the updating time of the proposed method and the recursive least square based method shown 22 by simulation. When running the machine at 500 rpm, the machine inductances L_d and L_q suddenly change from 45 mH to 47 mH, and from 102.7 mH to 132.7 mH, respectively. It is obvious that the proposed method results in an instant tracking of the inductance variation, while the method based of RLS algorithm takes about 0.5s to tracks the variation of the inductances.

The estimation accucy of the proposed method was experimentally compared with the off-line method [23] as shown in Fig. 11. For the whole range of the operating current from no load (0.25A) to 120% of rated load (3A) the results of two methods are closely matched. The root mean square error (RMSE) of the two methods for the direct axis inductance and quadrature axis inductance are 2.2 mH and 3.8 mH, respectively.

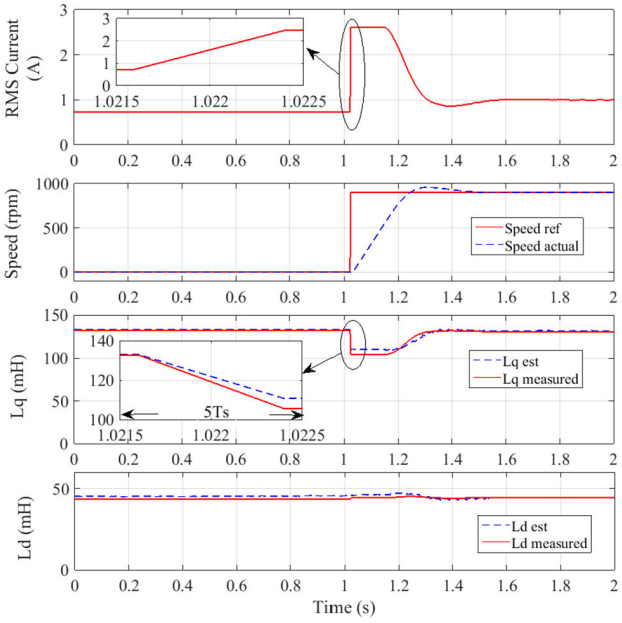

FIGURE 12. Inductances estimation during the speed acceleration from zero to 900 rpm (experiment).

The machine inductances are estimated by experiment when the machine accelerates from zero to 900 rpm as shown in Fig. 12. The estimated L_q is suddenly dropped from about 133mH to about 110 mH at the start of the acceleration (at time 1.05s), corresponding to the sudden increase of the RMS phase current from 0.9A to 2.8A. When the RMS phase current reduces to about 1.1A after the transient period, the estimated L_q increases to about 130mH. It is noted that during the transient the variation of the L_d is negligible. The comparison of the online estimated and the offline measured L_d and L_q during steady state and the transient state are also shown in Fig. 12. It is obvious that the online estimated inductances track very closely with the offline measured ones.

The results shown in Fig. 12 demonstrate the very fast inductances estimation (at PWM cycle as presented in section II) and zero speed operation capability of the proposed method.

IV. CONCLUSION

The paper has presented a sensorless control and online inductance estimation method for IPMSM based on current slopes during the excitation of one active and one zero voltage vector every PWM cycle. With the proposed sensorless method, the estimation accuracy is improved at low speeds and total harmonic distortion of the phase current is reduced over a full speed range, compared to the conventional FPE sensorless method, which utilizes two active and two zero volage vectors for sensorless performance. The measured current slopes at one active and one zero voltage vector are also utilized to estimate machine incremental and apparent direct and quadrature inductances. The high accuracy of the proposed online inductances estimation method during steady and fast transient states was verified by comparing

the estimated inductances with the values measured offline and RLS based online methods. The experimental results also verify the capability of proposed methods in estimating machine inductances during zero speed operation.

REFERENCES

[1] Z. Novak and M. Novak, "Adaptive PLL-based sensorless control for improved dynamics of high-speed PMSM," *IEEE Trans. Power Electron.*, vol. 37, no. 9, pp. 10154–10165, Sep. 2022, doi: 10.1109/TPEL.2022.3169708.

[2] X. Song, J. Fang, B. Han, and S. Zheng, "Adaptive compensation method for high-speed surface PMSM sensorless drives of EMF-based position estimation error," *IEEE Trans. Power Electron.*, vol. 31, no. 2, pp. 1438–1449, Feb. 2016, doi: 10.1109/TPEL.2015.2423319.

[3] F. Genduso, R. Miceli, C. Rando, and G. R. Galluzzo, "Back EMF sensorless-control algorithm for high-dynamic performance PMSM," *IEEE Trans. Ind. Electron.*, vol. 57, no. 6, pp. 2092–2100, Jun. 2010, doi: 10.1109/TIE.2009.2034182.

[4] D. Liang, J. Li, R. Qu, and W. Kong, "Adaptive second-order sliding-mode observer for PMSM sensorless control considering VSI nonlinearity," *IEEE Trans. Power Electron.*, vol. 33, no. 10, pp. 8994–9004, Oct. 2018, doi: 10.1109/TPEL.2017.2783920.

[5] A. T. Woldegiorgis, X. Ge, H. Wang, and Y. Zuo, "An active flux estimation in the estimated reference frame for sensorless control of IPMSM," *IEEE Trans. Power Electron.*, vol. 37, no. 8, pp. 9047–9060, Aug. 2022, doi: 10.1109/TPEL.2022.3156726.

[6] X. Qiu, J. Ji, D. Zhou, W. Zhao, Y. Chen, and L. Huang, "A modified flux observer for sensorless direct torque control of dual three-phase PMSM considering open-circuit fault," *IEEE Trans. Power Electron.*, vol. 37, no. 12, pp. 15356–15369, Dec. 2022, doi: 10.1109/TPEL.2022.3195495.

[7] T. Wu, D. Luo, X. Wu, K. Liu, S. Huang, and X. Peng, "Square-wave voltage injection based PMSM sensorless control considering time delay at low switching frequency," *IEEE Trans. Ind. Electron.*, vol. 69, no. 6, pp. 5525–5535, Jun. 2022, doi: 10.1109/TIE.2021.3094444.

[8] S. Wang, K. Yang, and K. Chen, "An improved position-sensorless control method at low speed for PMSM based on high-frequency signal injection into a rotating reference frame," *IEEE Access*, vol. 7, pp. 86510–86521, 2019, doi: 10.1109/ACCESS.2019.2925214.

[9] J. M. Liu and Z. Q. Zhu, "Novel sensorless control strategy with injection of high-frequency pulsating carrier signal into stationary reference frame," *IEEE Trans. Ind. Appl.*, vol. 50, no. 4, pp. 2574–2583, Jul. 2014, doi: 10.1109/TIA.2013.2293000.

[10] X. Luo, Q. Tang, A. Shen, and Q. Zhang, "PMSM sensorless control by injecting HF pulsating carrier signal into estimated fixed-frequency rotating reference frame," *IEEE Trans. Ind. Electron.*, vol. 63, no. 4, pp. 2294–2303, Apr. 2016, doi: 10.1109/TIE.2015.2505679.

[11] X. Luo, Q. Tang, A. Shen, H. Shen, and J. Xu, "A combining FPE and additional test vectors hybrid strategy for IPMSM sensorless control," *IEEE Trans. Power Electron.*, vol. 33, no. 7, pp. 6104–6113, Jul. 2018, doi: 10.1109/TPEL.2017.2743106.

[12] Y. Hua, M. Sumner, G. Asher, and Q. Gao, "Sensorless control for a PM machine with reduced current distortion using space vector PWM excitation," in *Proc. 13th Eur. Conf. Power Electron. Appl.*, Sep. 2009, pp. 1–10.

[13] Q. Gao, G. M. Asher, M. Sumner, and P. Makys, "Position estimation of AC machines over a wide frequency range based on space vector PWM excitation," *IEEE Trans. Ind. Appl.*, vol. 43, no. 4, pp. 1001–1011, 2007, doi: 10.1109/TIA.2007.900464.

[14] D. Q. Dang, M. S. Rafaq, H. H. Choi, and J. Jung, "Online parameter estimation technique for adaptive control applications of interior PM synchronous motor drives," *IEEE Trans. Ind. Electron.*, vol. 63, no. 3, pp. 1438–1449, Mar. 2016, doi: 10.1109/TIE.2015.2494534.

[15] T. Boileau, N. Leboeuf, B. Nahid-Mobarakeh, and F. Meibody-Tabar, "Online identification of PMSM parameters: Parameter identifiability and estimator comparative study," *IEEE Trans. Ind. Appl.*, vol. 47, no. 4, pp. 1944–1957, Jul. 2011, doi: 10.1109/TIA.2011.2155010.

[16] M. S. Rafaq, F. Mwasilu, J. Kim, H. H. Choi, and J. Jung, "Online parameter identification for model-based sensorless control of interior permanent magnet synchronous machine," *IEEE Trans. Power Electron.*, vol. 32, no. 6, pp. 4631–4643, Jun. 2017, doi: 10.1109/TPEL.2016.2598731.

[17] X. Li and R. Kennel, "General formulation of Kalman-filter-based online parameter identification methods for VSI-fed PMSM," *IEEE Trans. Ind. Electron.*, vol. 68, no. 4, pp. 2856–2864, Apr. 2021, doi: 10.1109/TIE.2020.2977568.

[18] W. Deng, C. Xia, Y. Yan, Q. Geng, and T. Shi, "Online multiparameter identification of surface-mounted PMSM considering inverter disturbance voltage," *IEEE Trans. Energy Convers.*, vol. 32, no. 1, pp. 202–212, Mar. 2017, doi: 10.1109/TEC.2016.2621130.

[19] M. X. Bui, D. Q. Guan, D. Xiao, and M. F. Rahman, "Sensorless control of interior permanent magnet synchronous motor based on the fundamental pulse width modulation excitation over a wide speed range," in *Proc. 19th Int. Conf. Electr. Mach. Syst. (ICEMS)*, Nov. 2016, pp. 1–6.

[20] A. Piippo, M. Hinkkanen, and J. Luomi, "Analysis of an adaptive observer for sensorless control of interior permanent magnet synchronous motors," *IEEE Trans. Ind. Electron.*, vol. 55, no. 2, pp. 570–576, Feb. 2008, doi: 10.1109/Tie.2007.911949.

[21] M. X. Bui, "Sensorless control and fast on-line parameter estimation of IPMSM based on current derivative measurements," Ph.D. dissertation, School Elect. Telecommun., Univ. New South Wales, Sydney, NSW, Australia, 2019.

[22] S. J. Underwood and I. Husain, "Online parameter estimation and adaptive control of permanent-magnet synchronous machines," *IEEE Trans. Ind. Electron.*, vol. 57, no. 7, pp. 2435–2443, Jul. 2010, doi: 10.1109/TIE.2009.2036029.

[23] R. Dutta and M. F. Rahman, "A comparative analysis of two test methods of measuring$d$- and$q$-axes inductances of interior permanent-magnet machine," *IEEE Trans. Magn.*, vol. 42, no. 11, pp. 3712–3718, Nov. 2006, doi: 10.1109/TMAG.2006.880994.

M. X. BUI (Member, IEEE) received the bachelor's degree in industrial automatic from the Hanoi University of Science and Technology, Vietnam, in 2005, and master's degree in electrical engineering from The University of Queensland, Australia, in 2010. He is currently a Lecturer with Le Quy Don Technical University, Vietnam. His research interests include power electronic and drive systems, and electrical machine designs.

DAN XIAO received the bachelor's and master's degrees in electrical engineering from the Shenyang University of Technology, Shenyang, China, in 2001 and 2004, respectively, and the Ph.D. degree in electrical engineering from the University of New South Wales (UNSW Australia), Sydney, Australia. He is currently a Technical Support with the Energy System Research Laboratories, UNSW Australia. His research interests include sensor-less control and online parameter estimation of ac machines, model predictive control for power converter and drives, matrix converters, and solid-state transformers.

M. FAZ RAHMAN (Life Fellow, IEEE) received the B.Sc. degree in engineering from the Bangladesh University of Engineering and Technology, in 1972, and the M.Sc. and Ph.D. degrees from The University of Manchester, U.K., in 1975 and 1978, respectively. He subsequently was a Systems Design Engineer with General Electric Projects Company, Rugby, U.K., for two years, and the National University of Singapore, Singapore, as a Senior Lecturer, for eight years. He is currently a Professor with the University of New South Wales, Australia. His research interests include power electronics, motor drives, and the design of electrical machines with PM excitation.